PCCP

PAPER

View Article Online
View Journal

Cite this: DOI: 10.1039/d6cp00537c

Molecular interactions in concentrated lithium sulfate solutions and their effect on electrochemical dissolution of iron

Hind A. Al-Malki[ab] and Katherine B. Holt *[a]

The electrochemical oxidation of an iron electrode to form dissolved Fe^{2+} was studied in a range of aqueous concentrated Li_2SO_4 solutions from 0.1 m to 2.5 m. The aim was to provide experimental understanding of molecular interactions in concentrated aqueous electrolytes and to determine whether these confer performance advantages for the all-iron redox flow cell anode reaction. Mass transport properties of the electrolyte solutions were probed through measurement of conductivity and determination of diffusion coefficients of dissolved probe species. Both methods showed an inhibition in species mobility above *ca.* 1 m, consistent with an increase in solution viscosity, loss of free water due to ion solvation and formation of ion pairs. Infra-red (IR) spectroscopy of the solutions showed a shift in wavenumber and asymmetry of the sulfate stretching peak as ion concentration increased, consistent with increasing ion–ion interactions. Distinctive changes to water IR bands were related to Li^+ solvation and formation of solvent separated ion pairs. Cyclic voltammetry was used to study Fe oxidation and dissolution in the electrolytes. Up until 1.8 m there was an increase in oxidation current as electrolyte concentration was increased, suggesting that use of concentrated electrolytes may be advantageous for this reaction. However above 1.8 m there was a suppression of current, confirmed by Raman spectroscopy to be caused by precipitation of $FeSO_4$ on the electrode as the saturation limit was reached. *In situ* IR spectroelectrochemistry was used to investigate the rate of Fe dissolution and the nature of solution molecular interactions as the reaction proceeded. An increase in SO_4^{2-} at the electrode surface was indicative of Fe dissolution producing Fe^{2+}, with the anion concentration increase proposed as balancing the local solution charge as the dissolved cation concentration increases.

Received 13th February 2026,
Accepted 11th May 2026

DOI: 10.1039/d6cp00537c

rsc.li/pccp

1. Introduction

Iron-based aqueous batteries are proposed as cheap and environmentally benign energy storage devices that can be operated under static or hybrid-flow conditions.[1–9] First discussed in detail by Hruska and Savinell in 1981,[5] there was little uptake by researchers until flow batteries began to be further developed about 30 years later. A drive to identify sustainable and less toxic redox reagents has led to renewed interest in Fe chemistry, particularly where reducing cost is important, such as off-grid applications.[6] In the simplest form, the all-iron aqueous battery consists of a negative half-cell with a Fe^0 electrode (anode) that on discharge releases Fe^{2+} into solution, along with electrons that transfer through the external circuit (E^0 = −0.44 V). The positive half-cell reaction is typically Fe^{3+} reduction to Fe^{2+} at a carbon electrode (E^0 = +0.77 V). The focus of this paper is the Fe^0/Fe^{2+} reaction at the anode (eqn (1)) and the effect of the electrolyte on the rate and products of the reaction, thus this introduction will focus on these aspects. The reader is directed towards reviews on different aspects of iron aqueous batteries, which include information on the cell construction, membrane properties and cathode reactions.[1–4]

$$Fe^0_{(s)} \rightarrow Fe^{2+}_{(aq)} + 2e^- \quad (1)$$

Various challenges exist around optimising the Fe^0/Fe^{2+} anode reaction.[7] In a full cell up to 50% of the voltage loss has been attributed to overpotentials associated with the iron electrode reaction, the $Fe^{2+/3+}$ reaction and membrane resistance making up the majority of the rest, at 27% and 14% voltage loss respectively.[5] The standard electrode potential for the reaction is −0.44 V which means, depending on the solution pH, reduction of protons or water can take place at the same potential leading to hydrogen production. The effect of pH has therefore been studied extensively, with a pH above 3 identified as optimum for prevention of hydrogen evolution.[5,9,10] However, a

[a] *Department of Chemistry, University College London, 20 Gordon St, London, WC1H 0AF, UK. E-mail: k.b.holt@ucl.ac.uk*
[b] *Department of Chemistry, College of Science, Umm Al-Qura University, P.O. Box 715, Makkah, 21955, Saudi Arabia*

pH above 7 should also be avoided to prevent the formation of iron oxides and hydroxides.[11] Hydrogen evolution is unwanted as it leads to lower coulombic efficiency, accumulation of gas bubbles and an increase in solution pH near the electrode which can cause precipitation of iron hydroxides.[9,10,12]

Common Fe solution redox species used are $FeCl_2$ and $FeSO_4$ with relatively high concentrations of 0.5–2.0 M reported as optimum.[5–7] From an environmental perspective the sulfate salt is preferred, as the chloride may be harmful to aquatic life,[6] however the conductivity of the chloride solutions is higher, which leads to faster Fe^0/Fe^{2+} electron transfer kinetics and better cell efficiencies.[5,6,10] Hydrogen evolution also seems to be suppressed in chloride relative to sulfate, perhaps due to strong chloride adsorption on the electrode.[10,13] For these reasons, most iron battery anode studies have focussed on optimising the $FeCl_2$ electrolyte system, for example by addition of supporting electrolytes. NH_4Cl was found to increase the solution conductivity and improve Fe stripping/plating kinetics, with no detrimental effects on the Fe deposit.[5,10] Supporting chloride electrolytes with different cations were also explored, with Li^+ and Na^+ resulting in faster rates of Fe stripping.[14]

As $FeSO_4$ is deemed more environmentally benign than $FeCl_2$ this paper focuses on understanding how electrolyte sulfate concentration influences the Fe oxidation reaction (eqn (1)). There are fewer prior studies using $FeSO_4$ rather than $FeCl_2$ in iron battery applications. Tucker *et al.* found that addition of NaCl or Na_2SO_4 supporting electrolytes was advantageous to performance of the Fe sulfate-based cell.[6] Likewise, NH_4Cl was added to $FeSO_4$ as an 'electrolyte regulator' to improve conductivity, kinetics and quality of the Fe electrode deposit.[15] Yu and co-workers used a 1-ethyl-3-methylimidazolium additive to increase the solubility of $FeSO_4$ and improve cell performance.[16] Wu *et al.* showed that the overpotential for Fe stripping in 0.5 M $FeSO_4$ at pH 5.5 was small (0.05 V), although the Coulombic efficiency for the Fe^0/Fe^{2+} reaction was low due to competing reactions such as hydrogen evolution.[8]

Recently there has been increased interest in the use of concentrated electrolytes in aqueous battery systems, where the availability of 'free' water is relatively low as most of the water is associated with solvation of ions.[17,18] The effect of this is to increase the overpotential required for the reduction (and oxidation) of water and so to require more negative potentials for hydrogen evolution to take place. The concentrated electrolyte under study in this paper is Li_2SO_4 at concentrations of 0.1–2.5 m and we focus on its effect on the Fe anodic dissolution (stripping) reaction (eqn (1)). In this work, an iron working electrode was used to produce Fe^{2+} through electrochemical dissolution. The Li_2SO_4 solutions used in this work mostly have pH values in the range below pH 7, so oxidation of metallic iron produces dissolved Fe^{2+}, as described in eqn (1), rather than oxides or hydroxides that would be formed above pH 7.[11] Moreover, it is known that $FeSO_4$ has relatively good solubility (above 1.5 M),[19] hence the use of the sulfate anion in the electrolyte should not interfere with this dissolution process. Out of the alkali metal sulfates, Li sulphate shows higher solubility (up to 2.5 M) compared to Na and K sulfate (solubility *ca.* 1 M) allowing a larger range of concentrations to be investigated. The other motivation for using a sulfate salt is that the anion is IR active meaning that it is an excellent probe for the IR spectroscopic and spectroelectrochemical studies reported herein.

This paper first describes the mass transport properties of the Li_2SO_4 electrolytes in isolation, using conductivity and diffusion coefficient measurements. IR spectroscopy is used to monitor changes to sulfate and water stretching bands as a function of electrolyte concentration; this allows information about molecular interactions in the solutions to be inferred. The electrochemical dissolution of Fe in the different solutions was measured using cyclic voltammetry (CV) and then monitored *in situ* using IR spectroelectrochemistry to determine the effect of electrolyte concentration on rate of Fe^{2+} formation.

2. Experimental

2.1. Characterisation of Li_2SO_4 solutions

All solutions were prepared using lithium sulfate monohydrate ACS reagent >99.0% (Sigma Aldrich) in ultrapure water of resistivity 18 MΩ cm produced from an Elga Purelab water purification system. Solutions were prepared using molality (m) rather than molarity (M) for the quantification of concentration. A fixed mass of water (typically 30 g) was added to the appropriate mass of salt and hence concentration is reported in units of mol kg^{-1}. The change in volume of the solutions on additional of salt was about 8% for the most concentrated solutions so the values of molality and molarity for the solutions deviate *e.g.* at 2.5 m the molarity of the solution is 2.3 M. These values are shown in Table S1 in SI. The solution pH values are also shown in Table S1 and vary from 7.03 at the lowest concentration (0.1 m) to 4.93 at the highest (2.5 m).

The electrical conductivity of Li_2SO_4 electrolyte at different concentrations was measured using a CDM230 Conductivity Meter with a traditional two-pole cell. The standard solution used for calibration in this experiment was 0.1 M KCl and the temperature was 293 K. IR spectroscopy of the different solutions was carried out using a Bruker Tensor 27 spectrometer with a diamond ATR prism. Spectra were measured for water and different concentrations of Li_2SO_4 after taking air as background. Difference spectra were obtained through subtraction of the spectrum of water from those of the Li_2SO_4 solutions.

2.2. Electrochemistry

The diffusion coefficient for 1 mM $K_4Fe(CN)_6$ dissolved in each of the different Li_2SO_4 concentration electrolytes was determined using cyclic voltammetry (CV) at six scan rates (10, 20, 50, 100, 200 and 500 mV s^{-1}) using a carbon working electrode of diameter 3.0 mm. A platinum coil electrode served as the counter electrode and Ag/AgCl electrode was used as the reference electrode. The oxidation peak currents of the resulting CV were used to determine the diffusion coefficient D of

$Fe(CN)_6^{4-}$ in each solution (see Section 3.1 and S3). To determine the effect of electrolyte concentration on Fe oxidation, CV measurements were carried out using a high-purity iron (Fe) wire (99.99%, Alfa Aesar) with a diameter of 1 mm as the working electrode. The sides of the wire were insulated with Teflon tape and a fresh electrode face exposed for each measurement using wire clippers. Experiments were repeated 3 to 5 times with a fresh electrode to evaluate reproducibility. All electrochemical measurements were performed using an EmStat3+ potentiostat controlled by PSTrace 5 software.

2.3. Raman spectroscopy

The measurements were performed *ex situ* using a Renishaw inVia Raman microscope equipped with a 514.5 nm laser, and spectral acquisition was controlled using WiRE 2 software. Raman spectra of the Fe electrode surfaces were recorded using 20 scans within the spectral range of 100–1300 cm^{-1}.

2.4. *In situ* spectroelectrochemistry

For *in situ* infrared (IR) spectroelectrochemical measurements, a three-electrode configuration was employed in a cell located above the ATR prism. A diagram of the cell is shown in S2 and its configuration and operation has been described previously.[20] The Fe working electrode was placed directly above the prism. The typical spacing between the electrode surface and ATR prism has been measured experimentally[21] as *ca.* 15 μm. As the IR evanescent wave penetrates about 1–2 μm (depth varies with wavenumber and solution refractive index) the region probed by the IR is within the diffusion layer but not directly at the electrode–solution interface. Initially, an IR spectrum was recorded with no potential applied to the Fe working electrode; this spectrum was used as the background reference. Subsequently, the potential was applied to the electrode, and IR spectra were recorded continuously. The spectra presented are therefore difference spectra, representing changes in the solution species in the region of solution located between the ATR prism and the iron electrode surface. The experiments were conducted under the same conditions for all Li_2SO_4 electrolyte concentrations.

3. Results and discussion

3.1. Characterisation of Li_2SO_4 aqueous electrolyte solutions: mass transport properties

Mass transport properties of the electrolyte solutions were probed through the measurement of conductivity (an indicator of ion mobility) and by determining the diffusion coefficient of a dissolved probe species.

Conductivity of the solutions as a function of Li_2SO_4 concentration is shown in Fig. 1a, where a consistent conductivity increase is observed between 0.1 m and 1.0 m. Above 1.0 m, conductivity increases more slowly with concentration before levelling off and slightly decreasing again at 2.5 m (although the values are within error bars for the latter data points). Also plotted on the figure are literature values measured at the same temperature,[22] which show the same trend but with a systematic offset to slightly lower values at the higher concentrations.

Fig. 1b shows the experimentally determined diffusion coefficient (D) values for ferrocyanide ($Fe(CN)_6^{4-}$) dissolved in aqueous Li_2SO_4 solutions of different concentrations. CVs for ferrocyanide at a concentration c of 1 mM were recorded at a range of scan rates ν. The peak oxidation currents i_p^{ox} were then used to determine D using the Randles–Ševčik equation (eqn (2)), assuming that T = 298 K:

$$i_p^{ox} = (2.69 \times 10^5) n^{3/2} A D^{1/2} c \nu^{1/2} \quad (2)$$

where n is the stoichiometric number of electrons transferred (in this case 1) and A is the area of the electrode. In using this equation, electron transfer kinetics are assumed to be reversible; however, it is known that the ferro/ferricyanide redox couple often exhibits quasireversible behaviour.[23] Experimentally we found that CV peak separations of 80 mV were observed over all electrolyte concentrations from 1 m and above, with peak separation being independent of scan rate (Fig. S2). Although the CVs are not fully reversible in terms of peak

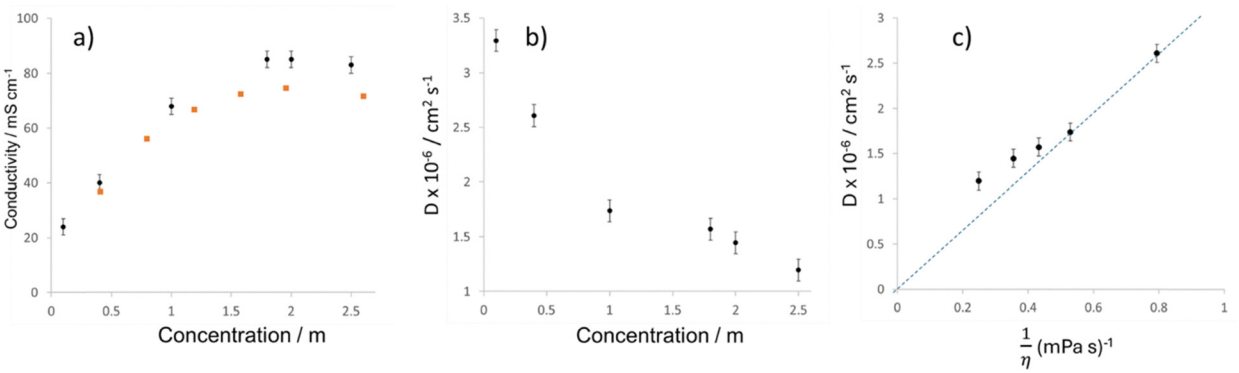

Fig. 1 (a) Conductivity of Li_2SO_4 aqueous solutions as a function of concentration (T = 293–297 K) black circles are experimental values from this study with errors determined from typical range of three measurements on different days; orange squares are literature values from ref. 2; (b) diffusion coefficient, D, for 1 mM $Fe(CN)_6^{4-}$ dissolved in Li_2SO_4 solutions of different concentrations. D determined from analysis of cyclic voltammograms using eqn (2) (see S3); (c) experimentally obtained values of D for $Fe(CN)_6^{4-}$ plotted against reciprocal of solution viscosity (η). Values of η for the different concentration Li_2SO_4 solutions obtained from ref. 22. Dashed line is a guide to the eye for a linear Stokes–Einstein relationship in dilute solutions (eqn (3)).

separation there was no dependence of kinetics on electrolyte concentration. Hence for the purposes of determining trends in D values as a function of electrolyte concentration eqn (2) allows an adequate approximation. Fig. 1b shows D values of 1–3.5 $\times$ 10^{-6} cm^2 s^{-1} are obtained, which are of similar magnitude but about half the literature values obtained in 0.1 and 1.0 m KCl electrolytes.[24] There is a significant decrease in D between 0.1 m and 1 m Li_2SO_4 electrolyte, with values levelling off and decreasing more gradually at the higher concentrations.

Taken together, Fig. 1a and b suggest a change in solution mass transport properties between lower concentrations (1.0 m and below) and higher concentrations (1.8 m and above). From 0.1 m to *ca.* 1.0 m the ions exert a cumulative effect on the properties of the solution. Conductivity increases consistently, although not linearly, in this range as more charge carriers are available to carry current. At 1.8 m and above the conductivity reaches an almost constant value and does not increase as more ions are added. Likewise, over the 0.1 m to 1.0 m concentration range the D value for dissolved ferrocyanide shows a cumulative decrease as more ions are added. However, at 1.8 m and above a similar levelling off the mobility of the dissolved redox probe is observed. This represents a significant inhibition in both ion mobility and diffusion of dissolved species that could be attributed to an increase in solution viscosity and/or the formation of ion pairs.

According to the Stokes–Einstein equation (eqn (3)) there is a reciprocal relationship between D and solution viscosity η:

$$D = \frac{k_B T}{6\pi R\eta} \quad (3)$$

where R is the hydrodynamic radius of the diffusing species. Fig. 1c shows the experimentally obtained D values plotted against $1/\eta$, where the viscosity values of the relevant solutions were obtained from literature (Table S2).[22] A linear relationship with a zero-intercept is expected if eqn (3) is valid; however, Fig. 3c shows a deviation from this relationship in solutions above 1 m concentration. The form of the Stokes–Einstein equation with the constant 6 in the denominator is valid for dilute solutions where the diffusing species is of much larger dimensions than surrounding molecules ('no-slip' conditions). When molecules in the surrounding media are of a similar size to the diffusing molecule, or when there are extensive molecular interactions, a denominator constant of 3 or 4 is needed to describe the observed relationship ('slip' conditions).[25] In Fig. 1c for the higher concentration (higher viscosity) solutions the experimental D values obtained lie higher than predicted by eqn (3), which is consistent with these solutions falling within the 'slip' regime.

The change in diffusion behaviour suggests that the 1.8 m, 2.0 m and 2.5 m solutions may exhibit ion-pairing forming larger dimension entities in solution than the fully hydrated ions present at lower concentrations. Likewise, ion-pairing, as well as an increase in solution viscosity can explain the observed experimental conductivity values. As ion pairs often exhibit a dipole, they can respond to an external electric field; however, they do not contribute to measured conductivity to the same extent as migrating free ions. A levelling-off of measured conductivity at high concentrations is therefore indicative that ion association is taking place. Ion pairs can be contact ion pairs (CIPs), where opposite charged ions share a solvation shell, or solvent separated ion pairs (SSIPs) in which the ions are associated electrostatically but with a layer of solvent separating them.[25] Previous studies have proposed that SSIPs predominate over CIPs in Li_2SO_4 solutions.[26]

3.2. Structural properties of Li_2SO_4 aqueous electrolyte solutions: IR spectroscopy

To probe the electrolyte structure, the ATR-IR spectrum of each solution was recorded, with absorption spectra for the sulfate ion asymmetric stretch (ν_3) shown in Fig. 2a. At 0.1 m and 0.4 m Li_2SO_4 the peak is symmetrical and centred at *ca.* 1100 cm^{-1}. At 1.0 m concentration the peak maximum shifts to 1092 cm^{-1} and exhibits a shoulder to the higher wavenumber side. This is shown more clearly in Fig. 2b, where the peaks have been normalised to their maximum absorbance values and overlaid. Above 1.0 m there continues to be a small shift towards lower wavenumbers with increasing concentration and a clear asymmetry to the peak.

One explanation for the shift in peak position is a vibrational Stark effect, due to the increased electric field experienced by the sulfate ions as the density of ions in the solution increases.[27] Typically, the dipole moment of a molecule is different in the ν = 0 and ν = 1 vibrational states, due to anharmonicity, so differing degrees of destabilisation are experienced by the ground and excited vibrational states in the presence of an electric field, such as that generated collectively by the solvated ions. Hence the energy gap between the vibrational states is altered, resulting in a shift in wavenumber for the fundamental transition. A second explanation for the observed peak shift is an increase in ion pairing between the SO_4^{2-} and Li^+ ions as the space between neighbouring ions decreases. This can perturb the sulfate tetrahedral geometry by removing the equivalence of the oxygen atoms, causing splitting and broadening of the peak and a shift in peak maximum.[28] Both explanations are related to neighbouring ions exerting an increased effect on each other as concentration is increased, with the most dramatic changes being observed between 0.4 m and 1.0 m. This suggests that the most profound change in electrolyte ionic atmosphere takes place over this concentration range, while the effect of adding more ions becomes more incremental at higher concentrations.

Fig. 2c shows the water stretching absorption bands (2600–3800 cm^{-1}) for pure water and the Li_2SO_4 solutions at different concentrations. The strong, broad bands show a small and cumulative increase in intensity as the ion concentration is increased, especially towards the lower wavenumber side of the peak maximum. There is also a slight broadening to the lower wavenumber side of the peak. Difference spectra are presented in Fig. 2d, where the spectrum for pure water has been subtracted from the spectrum of each salt solution, to better reveal the effect of electrolyte ions on the water bands. In all cases, a positive change in absorbance is observed from

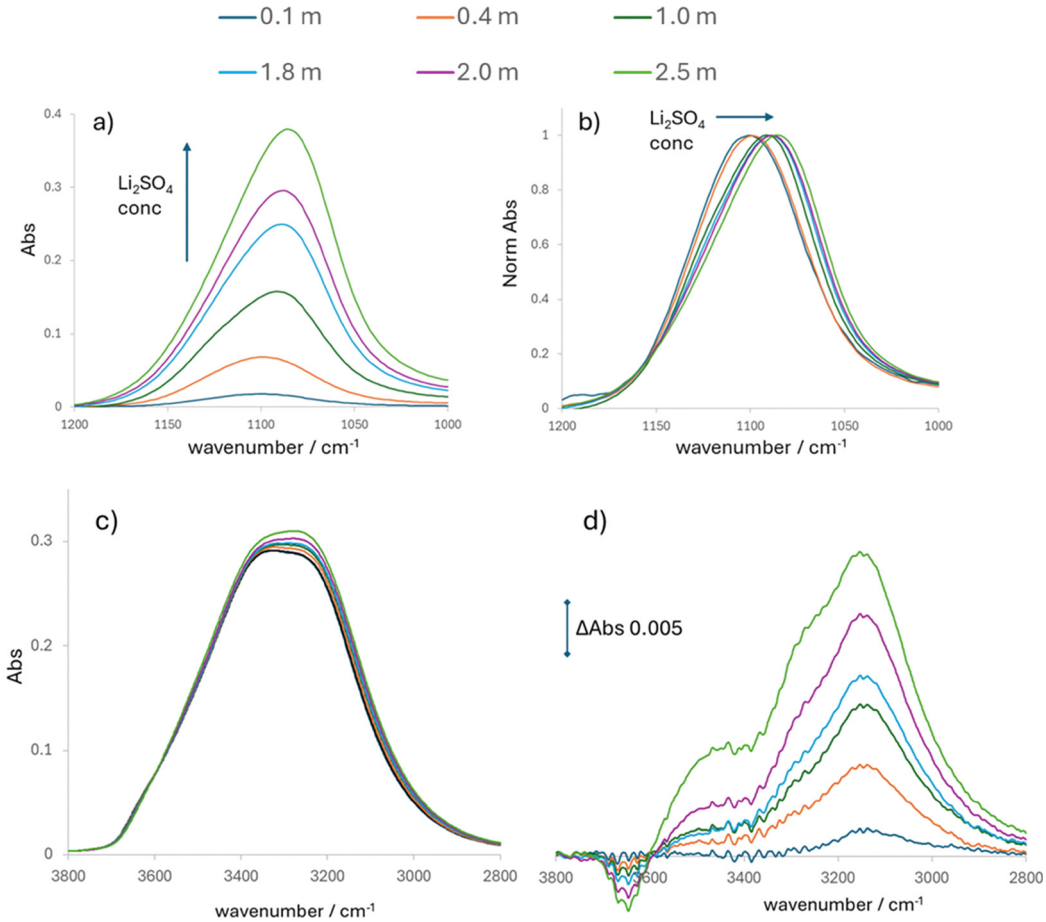

Fig. 2 ATR-FTIR spectra of different concentrations of Li_2SO_4 in water: 0.1 m (dark blue); 0.4 m (orange); 1.0 m (dark green); 1.8 m (light blue); 2.0 m (purple) and 2.5 m (light green); (a) absorption spectra of sulfate asymmetric stretch (ν_3) region; (b) normalised absorption spectra of sulfate asymmetric stretch normalised to 1 for the maximum abs values; (c) absorption spectra for the water symmetric and asymmetric stretch region; (d) difference spectra for the water symmetric and asymmetric stretching region, where the spectrum for pure water has been subtracted from each Li_2SO_4 electrolyte spectrum.

ca. 2900–3600 cm^{-1}, with a maximum at 3147 cm^{-1} that increases with salt concentration. Clear shoulders are seen at 3275 cm^{-1} and 3445 cm^{-1}. A decrease in absorbance as a function of salt concentration is noted at 3643 cm^{-1}.

The IR spectra of the water stretching region for Li_2SO_4 solutions has been reported previously, with similar results to Fig. 2c and d.[29] Interpretation is simplified by classification of the sulfate ion as a 'blank anion' that has been demonstrated to have little effect on the IR stretching bands of water.[30,31] Thus, changes to the water bands can be attributed solely to the solvation of the Li^+ ion. On addition of Li^+ an increase in absorption towards the lower wavenumber values for water (2900–3600 cm^{-1}) is observed and typically attributed to a greater degree of hydrogen-bonding between neighbouring water molecules in the Li^+ solvation shell.[29] The decrease in absorbance at 3643 cm^{-1} is associated with a loss of 'free' non-hydrogen bonded water.

It might be expected that the changes in absorption should be additive with salt concentration but previously it has been noted that a linear relationship only exists for concentrations of Li_2SO_4 up to 0.5 M.[25] This is also observed in this work, as shown in Fig. 2d, where above 0.4 m ΔAbs at 3147 cm^{-1} does not increase in proportion to Li^+ concentration. This non-linearity is apparently a unique property of Li_2SO_4 solutions as, in contrast, it is reported that LiCl solutions at the same molarity of Li^+ do show a linear relationship between ΔAbs at 3147 cm^{-1} and Li^+ concentration.[29]

Fig. 2d also shows the emergence of a shoulder at 3445 cm^{-1} which has a non-linear concentration dependence of ΔAbs. The band at 3445 cm^{-1} has previously been reported for Li_2SO_4 solutions but not LiCl solutions over the same concentration range.[29] This suggests that while the sulfate ion is a 'blank anion' that does not influence the water IR features itself, it does exert an effect on Li^+ that results in distinctive features for the Li_2SO_4 solutions specifically. A proposed origin for this unique water absorption feature was a cooperativity in ion hydration, an effect observed for strongly hydrated cations and anions sharing an aqueous solution.[32] Here, the water molecules beyond the first solvation layer are influenced by both anion (SO_4^{2-}) and cation (Li^+) and they become partly 'locked' in a specific orientation between the two, with restricted motion. This 'locked' water is consistent with the

formation of SSIP in Li_2SO_4 solutions and its presence may be indicated by the feature at 3445 cm^{-1}.

The IR spectra for both sulfate and water show that a change in anion and water environment is experienced as the concentration of the Li_2SO_4 solutions is increased. In particular, evidence of cation–anion interaction, likely a form of ion-pairing is noted at 1.0 m and above. The bonding environment of water is also changed. These results are consistent with the changes in the conductivity and diffusion coefficient values over the same concentration ranges, as described above.

2.3. Voltammetry of an Fe electrode in Li_2SO_4 aqueous electrolyte solutions

Cyclic voltammetry (CV) was used to study the effect of electrolyte concentration on Fe oxidation and dissolution. Fig. 3 shows the forward scan CV responses for the fifth consecutive scan of an iron electrode in different concentrations of Li_2SO_4 electrolyte. Complete CVs can be seen in Fig. S4. The CV response was found to change over consecutive scans, with the current increasing with continued cycling (see Fig. S6). Therefore, for consistency the fifth scan in each solution has been compared. The increase in current with cycling is likely due to increased electrode surface area and roughening with each stripping and deposition cycling. During the first scan the smooth, newly exposed Fe surface undergoes oxidation and dissolution, requiring a large activation energy and resulting in smaller currents. During reduction, the dissolved Fe^{2+} is redeposited onto the surface, most likely *via* a nucleation and growth process, rather than smooth plating. Therefore, the Fe surface will roughen with increased cycling and develop a larger surface area of more reactive Fe deposits than the original surface, resulting in larger currents.

For the lowest concentration of 0.1 m the onset of the oxidation current is seen at *ca.* −0.4 V. The standard potential is −0.67 V *vs.* Ag/AgCl so the reaction has an observed overpotential of *ca.* 0.24 V. At Li_2SO_4 concentrations of 0.4 M and above, the onset of the oxidation shifts to less positive potentials and is consistently much closer to the standard potential, indicating enhanced electron transfer kinetics. The oxidation current achieved at −0.4 V is plotted against electrolyte concentration in the Fig. 3 inset, showing an initial continuous increase until 1.8 m, followed by a levelling off or slight decrease. If current magnitude is taken as dissolution reaction rate, then dissolution happens faster as ion concentration is increased, until a limit is reached above 1.8 m.

The shape of the CV current response also changes as function of electrolyte concentration. At lower electrolyte concentrations, the oxidation current consistently increases as the potential is swept towards 0.1 V. This is the response expected for a solid electrode undergoing continuous dissolution in this potential range. At 1.8 m the current response becomes distinctly peak-like. At 2.0 and 2.5 m the highest currents achieved are lower than those at 1.8 m and the current reaches a maximum at −0.05 V before rapidly decreasing. The symmetrical form of the peak response and the rapid decay in the current is very characteristic of a reaction involving surface passivation. Thus, it seems that at 1.8 m Li_2SO_4 and above the initial fast dissolution of Fe is followed by subsequent chemical processes that partially block the surface and prevent further oxidation. This is discussed further in Section 3.4 below.

The currents for the oxidation process increase approximately linearly from 0.1 m to 1.8 m Li_2SO_4 concentration; hence it is instructive to consider which properties of the solution may have an influence on this observed increased rate. From Fig. 1a, the solution conductivity increases in this concentration range. It has been reported previously that increasing electrolyte conductivity is an essential factor for

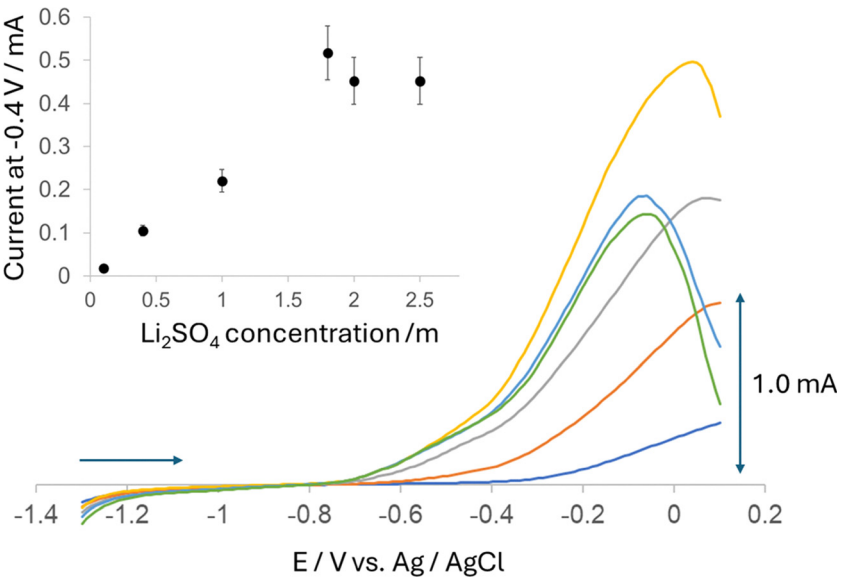

Fig. 3 Forward scan of fifth consecutive CV for iron electrode (area 7.85 × 10^{-3} cm^2) in different concentrations of Li_2SO_4 electrolyte: dark blue 0.1 m; orange 0.4 m; grey 1.0 m; yellow 1.8 m; light blue 2.0 m and green 2.5 m. Scans start at −1.3 V and sweep in the positive direction. Inset: Oxidation current at −0.4 V as a function of Li_2SO_4 electrolyte concentration.

maximised coulombic efficiency and energy density for the all-iron redox flow cell as this improves the kinetics and reversibility for the Fe^0/Fe^{2+} redox reaction.[5–7,10,14,15] The relationship of dissolution rate to conductivity may be due to the increased number of mobile solution ions, in particular anions, available to stabilise the Fe^{2+} product in solution. In particular, ion pairing between Fe^{2+} and SO_4^{2-} in water is quite significant, with reported ion association constant of 158.49 M^{-1},[33] contrasting with an ion association constant of 6–7 M^{-1} for Li_2SO_4.[26] The favourable interaction between Fe^{2+} and excess sulfate may therefore be a driver for the increased dissolution currents observed as the electrolyte concentration increases. The IR spectra of the Li_2SO_4 solutions showed evidence of ion–ion interactions and SSIP formation at concentrations of Li_2SO_4 above 0.4 m. These interactions do not, however, appear to prevent the effective dissolution of Fe^{2+} into an already ion-dense solution. Although a great deal of the water in these solutions is already either bound directly to electrolyte ions, or influenced by ionic electric fields, there seems to be sufficient dynamic freedom to allow free dissolution of Fe^{2+} at a high concentration near the electrode interface, at least up to a Li_2SO_4 concentration of 1.8 m. The rate of this dissolution process and the interactions between Fe^{2+}, sulfate and water are investigated further using *in situ* IR spectroelectrochemistry in Section 3.5.

Although over the same concentration range the diffusion coefficient of dissolved species decreases (Fig. 1b), which suggests that solution viscosity is increasing, this does not seem to detrimentally affect the oxidation currents for Fe dissolution. This makes sense, given that the dissolution reaction does not depend on mass transport of solution species towards the electrode, as the electrode itself is the reactant, so the reaction is not under diffusion-control. The increased solution viscosity might however adversely affect the reverse Fe^{2+} reduction reaction rate, as this involves as diffusing species (this was beyond the scope of the current study).

2.4. Raman spectroscopy of iron surface after oxidation

The observed decrease in Fe oxidation rate at Li_2SO_4 concentrations of 2.0 m and 2.5 m and the peak shaped CV responses are suggestive of the formation of a non-conductive passivating layer on the Fe surface at potentials above −0.1 V *vs.* Ag/AgCl. Iron oxide or hydroxide formation is not predicted to occur at potentials below 0.2 V *vs.* Ag/AgCl at the pH used in this study so further characterisation is required to understand this observation.[11]

To investigate the observed surface passivation, iron electrodes were held at −0.1 V (close to the potential of the peak maxima observed in Fig. 3) for 300 s in each of the different electrolyte solutions. The surface of the dried electrode was then characterised *ex situ* using Raman spectroscopy to observe any resulting films. As shown in Fig. 4, after treatment in 0.1, 0.4 and 1.0 m electrolyte the electrode surface showed only very weak Raman features, indicating very little change to the surface. This is consistent with the lack of current passivation observed. After treatment in 1.8 m a sharp, strong peak is present at 1008 cm^{-1}. At higher concentrations of 2.0 m and 2.5 m the same strong peak is seen at 1008 and 1011 cm^{-1} respectively, along with sequential small peaks from 1105 to 1182 cm^{-1}. The presence of the peaks indicates that a solid surface film has formed after treatment at −0.1 V and this is likely the cause of the current deactivation seen in the CVs.

The Raman spectra of the films are very similar to those reported for iron sulfate materials.[34] The symmetrical, non-complexed SO_4^{2-} ion has four Raman active vibrational modes: ν_1 (983 cm^{-1}, symmetric stretching), ν_2 (450 cm^{-1}, symmetric bending), ν_3 (1105 cm^{-1}, asymmetric stretching) and ν_4 (611 cm^{-1}, asymmetric bending). The strong peak observed in

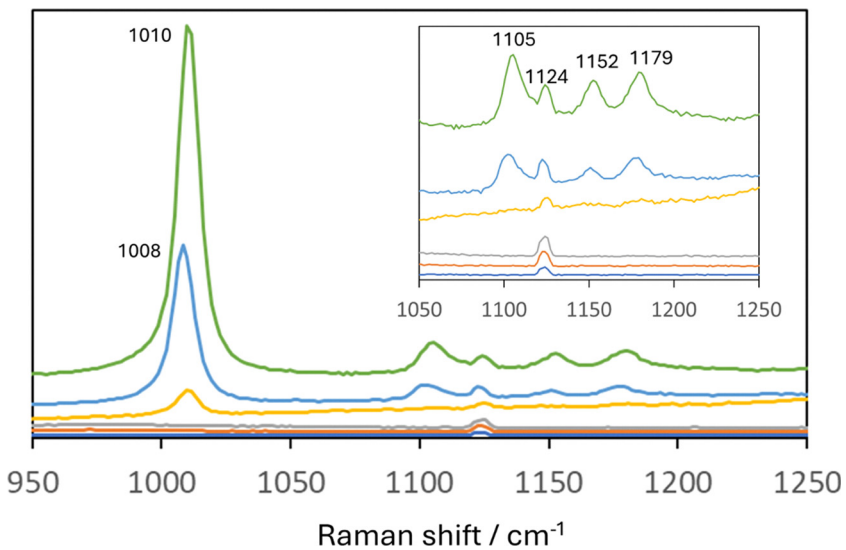

Fig. 4 *Ex situ* Raman spectra (514.5 nm laser) of the surface of Fe electrodes after treatment at −0.1 V in different concentration solutions of Li_2SO_4: 0.1 m dark blue; 0.4 m orange; 1.0 m grey; 1.8 m yellow; 2.0 m dark blue and 2.5 m green. The inset shows a magnified view of the 1050–1250 cm^{-1} region representing the split peaks for the ν_3 mode (see text).

Fig. 4 at 1008–1011 cm^{-1} indicates the symmetric vibrational mode ν_1 of SO_4^{2-}, which gives sharp and intense Raman lines. This mode has been reported to show an increase in wavenumber as the amount of water incorporated into the iron sulfate structure decreases, hence hepta-, tetra-, and monohydrates of $FeSO_4$ have a ν_1 peak at 976, 990 and 1018 cm^{-1}, respectively. The films in Fig. 4 are consistent with the least hydrated solids, as might be expected for the high electrolyte concentrations used, where there is little water available to incorporate into the solid material.

Peaks are also observed for the asymmetric vibrational mode ν_3 at 1105–1179 cm^{-1}, which is split into four peaks for the 2 and 2.5 m treated samples at 1105, 1124, 1152 and 1179 cm^{-1} (see inset to Fig. 4). The distribution and positions of the peaks are similar, although not identical to those reported for pure hepta-, tetra-, and monohydrates of $FeSO_4$.[34] The splitting of the peak results from decreased symmetry of the sulfate and indicates a range of bonding interactions between the anion and cation. Taken together the Raman peaks show that significant deposition of iron sulfate occurs when the concentration of Fe^{2+} and SO_4^{2-} are high, adjacent to the electrode surface. When the upper limit of iron sulfate solubility is reached, the solid is precipitated on the electrode, thus creating a passivation layer on the surface. The solubility of $FeSO_4{\cdot}7H_2O$ is 1.7 mol dm^{-3} at 20 °C,[19] which is consistent with the film deposition being observed at electrolyte sulfate concentrations of 1.8 m and above.

As expected from the potentials used in this study, the Raman spectra show no evidence of oxide or hydroxide species deposited on the electrode surface.

2.5. *In situ* IR spectroelectrochemistry of the iron electrode–electrolyte interface

To monitor the iron anodic dissolution process, *in situ* IR spectroelectrochemistry experiments were carried out using the arrangement shown in Fig. 5a and Fig. S2. A three-electrode cell was mounted on top of an ATR prism, with the Fe working electrode located directly above the sampling region of the IR beam, where the evanescent wave penetrates the solution above the prism. Different potentials were applied to the Fe electrode and changes to the IR spectrum at the electrode–electrolyte interface were measured as a function of time and in Li_2SO_4

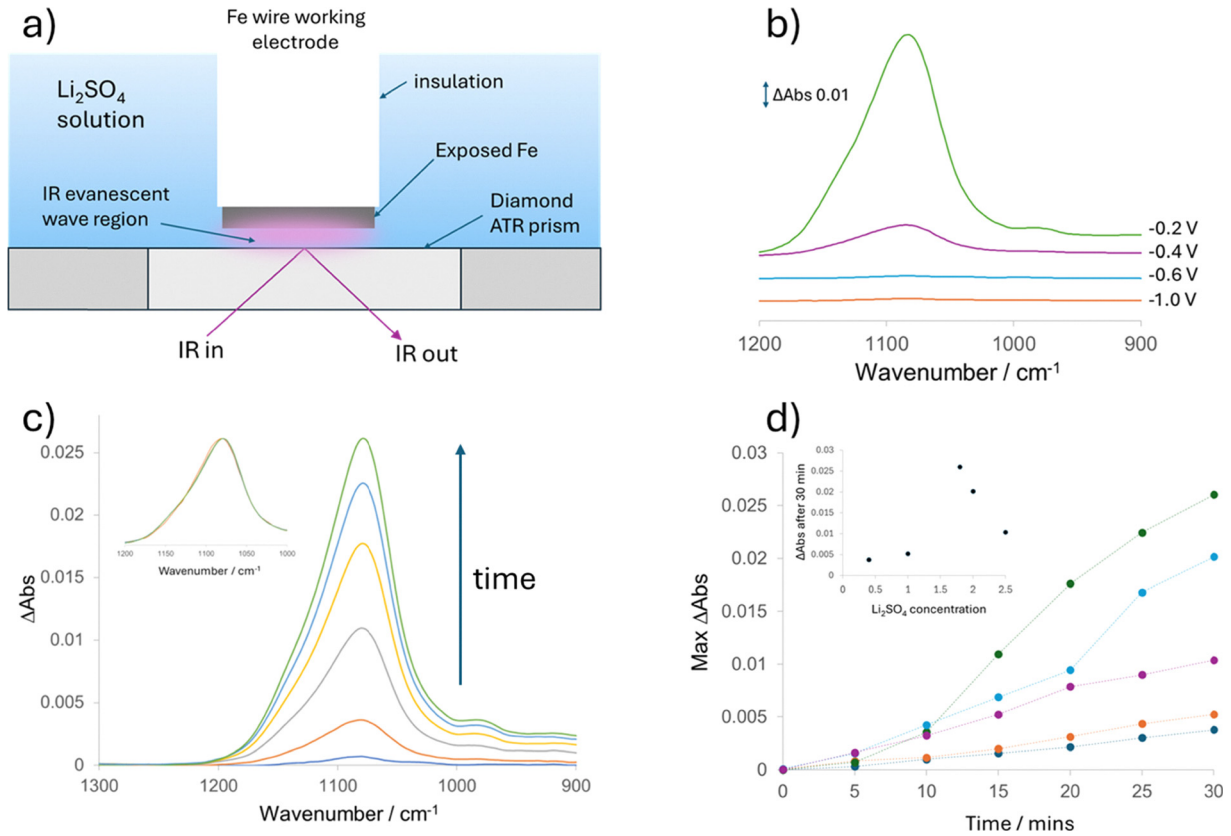

Fig. 5 (a) Schematic (not to scale) of the Fe electrode located above the ATR IR prism for *in situ* spectroelectrochemical measurements in Li_2SO_4 solutions of different concentration. The evanescent IR wave probes the electrode–electrolyte interfacial region; (b) difference IR spectra showing change to the sulfate band after 20 min in 1.0 m Li_2SO_4 with different potentials applied to the Fe working electrode, spectra are measured relative to the spectrum at no applied potential; (c) changes to IR sulphate band as a function of time after application of −0.4 V to the Fe electrode in a solution of 1.8 m Li_2SO_4: each spectrum recorded at 5 min increments for 30 min. Inset shows the spectra normalised to an absorbance of 1 at the peak maximum and overlaid; (d) maximum ΔAbs of the sulfate band as a function of time after application of −0.4 V in different Li_2SO_4 solutions: 0.4 m dark blue; 1.0 m orange; 1.8 m green; 2.0 m light blue; 2.5 m purple. Lines between data points are solely to guide the eye. Inset shows the ΔAbs after 30 min as a function of Li_2SO_4 electrolyte concentration.

solutions of different concentration. Spectral changes in 0.1 m solution were too small to be reliably monitored, so only the results in higher concentrations are reported here.

Fig. 5b shows IR difference spectra measured 20 min after application of different potentials to the Fe electrode in a 1.0 m Li_2SO_4 solution. First a spectrum of the interface without applied potential was measured and this was subtracted from subsequent spectra measured at different times after the potential was applied. Hence the spectra show changes to the solution species as a result of the potential applied to the Fe electrode. At potentials of −1.0 V and −0.6 V there is negligible change to the spectra after 20 min but at −0.4 V an increase in absorption is seen in the sulfate region with a peak maximum of 1084 cm^{-1}. At −0.2 V this difference peak is significantly more intense, with a maximum at 1082 cm^{-1} and asymmetry and broadening to the higher wavenumber side.

Comparison of these spectra to the CV responses in Fig. 3 shows that significant changes to the IR absorbance are only seen when currents for Fe oxidation concurrently occur. At −1.0 V the potential is negative of the standard potentials for the Fe^0/Fe^{2+} redox reaction so no current flows, while at −0.6 V, close to the standard potential, the current is very small as the oxidation kinetics are relatively slow in 1.0 m electrolyte solution. The lack of change in the IR difference spectra is consistent with no or little reaction taking place at −1.0 and −0.6 V. At −0.4 V Fe oxidation occurs at a measurable rate and the current increases still further at −0.2 V, where Fe^{2+} formation is very fast. This is reflected in the significant changes in the IR spectra at these potentials, with the ΔAbs increase being larger at −0.2 V than −0.4 V.

The change in IR absorbance with time at −0.4 V is shown in Fig. 5c for the Fe electrode immersed in 1.8 m Li_2SO_4 solution. The asymmetric sulfate band with a maximum at 1078 cm^{-1} increases in absorbance consistently, although not linearly, with time. The inset to Fig. 5c shows the peaks at different times normalised to absorbance of 1 at the peak maximum and overlaid, where it can be seen that the shape and position of the peak does not change over 30 min. Similar spectra were recorded over 30 min for Fe at −0.4 V in the 0.4 m, 1.0 m, 2.0 m and 2.5 m Li_2SO_4 solutions and are shown in S7. Fig. 5d shows the maximum ΔAbs of the sulfate peak as a function of time for the different Li_2SO_4 concentrations where, by comparing the inset of Fig. 4 with the inset of Fig. 5d, a relationship can be seen between the maximum currents achieved at −0.4 V and the values of ΔAbs after 30 min. The increase in IR absorbance for the solution sulphate species therefore appears to be correlated to the quantity of Fe^{2+} generated at the electrode interface.

It is proposed that the observed increase in the sulfate absorbance is due to the local increase in cationic Fe^{2+} species requiring a balancing of charge through flux of sulfate anions to this interfacial region. Hence an increase in sulfate concentration is observed as the Fe^{2+} concentration increases. The wavenumber of the sulfate peak maximum is shifted to lower values than observed in the corresponding Li_2SO_4 solution, as shown in Fig. 6a. Here, the normalised *in situ* spectrum in 1.8 m Li_2SO_4 at 30 min after application −0.4 V (thick black; max. 1078 cm^{-1}) has been overlaid with a normalised absorption spectrum for a 1.8 m Li_2SO_4 solution (dashed black; max. 1090 cm^{-1}). Also included is a normalised spectrum obtained from the subtraction of the spectrum for 1.8 m Li_2SO_4 from the spectrum of a mixture of 1.8 m Li_2SO_4 + 0.15 m $FeSO_4$ (red; max. 1083 cm^{-1}), which shows that addition of Fe^{2+} to a Li_2SO_4 solution results in absorption increases to the lower wavenumber side of the sulfate bands. This supports the proposal that the increase in absorption associated with sulphate is an indirect indicator of increased Fe^{2+} in the solution region being probed. Further support is given by comparing the water absorption region for these three solutions (normalised to the sulfate peak maximum) as shown in Fig. 6b. Here the water difference spectrum for the $FeSO_4$ containing solution (red) shows almost identical spectral features to the *in situ* spectrum at the electrode interface (thick black). Both spectra are very different from that obtained for the solution containing only Li_2SO_4 (black dashed) which further supports that changes to the IR spectra for both sulfate and water are strongly correlated with the presence of Fe^{2+}.

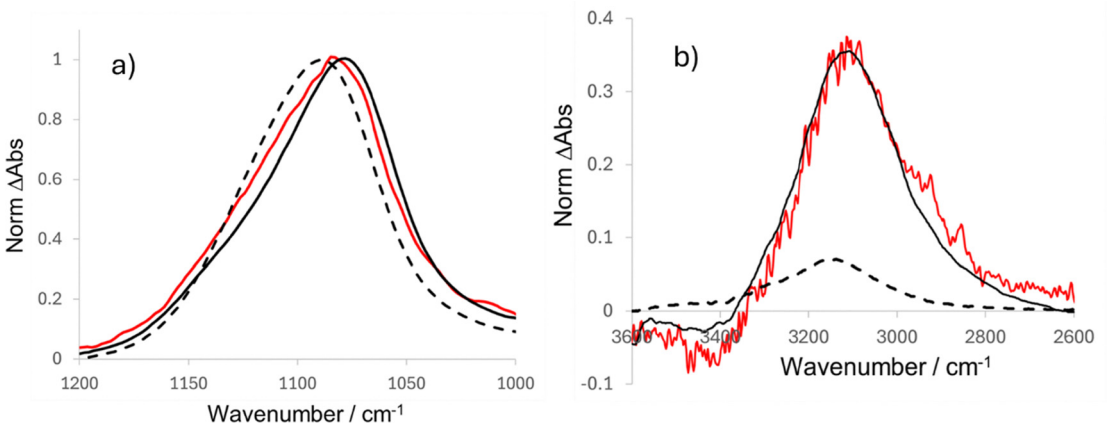

Fig. 6 Difference IR spectra normalised to 1 at peak maximum for sulfate band. Dashed = 1.8 m Li_2SO_4; solid black = *in situ* spectrum at Fe electrode surface obtained in 1.8 m Li_2SO_4 after 30 min at −0.4 V; red = spectrum obtained from subtraction of 1.8 m Li_2SO_4 spectrum from that of mixture of 1.8 m Li_2SO_4 + 0.15 m $FeSO_4$; (a) sulfate asymmetric stretch region; (b) water stretching region.

4. Discussion and conclusions

The iron stripping reaction related to the anode reaction of the all iron-redox flow battery was studied here in aqueous concentrated Li_2SO_4 solutions from 0.1 m to 2.5 m, to determine whether high concentration electrolytes confer performance advantages and improve electron transfer kinetics. It was found that up to about 1.8 m the currents for the Fe^0/Fe^{2+} oxidation increased significantly with electrolyte concentration, demonstrating an increased dissolution rate. The onset potential for the reaction also shifted towards lower overpotentials, suggesting improved kinetic performance. However, increasing the electrolyte concentration further resulted in currents becoming limited and passivated as the solubility limit for the $FeSO_4$ product was reached. Raman spectroscopy confirmed the presence of $FeSO_4$ films on the electrode surface under these conditions. Thus, it can be concluded that from an application perspective, high electrolyte concentrations should be explored but advantages may only be observed over specific concentration ranges depending on the electrolyte composition.

The fundamental properties of the Li_2SO_4 electrolytes were explored to gain insight into the molecular interactions responsible for the solution properties and how these might relate to electrolyte performance in this application. Solution conductivity increased rapidly up to 1 m, with a further small increase to 1.8 m followed by levelling off or decline. The correlation between conductivity and the rate of Fe dissolution suggests that availability of mobile electrolyte ions is a dominating factor in explaining the improved electrochemical performance. Dissolution is clearly favoured when more solution anions are available to interact with and stabilise the Fe^{2+} cation product, potentially driven by the high propensity of Fe^{2+} and SO_4^{2-} to ion pair. This conclusion was supported by *in situ* IR spectroelectrochemistry, where a measured increase in SO_4^{2-} at the electrode surface was taken as indicative of Fe^{2+} dissolution, with the anion concentration increase proposed as balancing the local change in solution charge as the dissolved cation concentration increases.

The levelling off of the conductivity at concentrations 1 m and above may be indicative of ion pairing in the solution occurring in the solution at this concentration and above. Further evidence for these molecular interactions was obtained from measurement of diffusion coefficients of a dissolved probe species. This method showed an inhibition in species mobility above *ca.* 1 m, that could only partly be attributed to increased viscosity. IR spectroscopy of the solutions also showed a shift in wavenumber and asymmetry of the sulfate stretching peak as, over this same concentration range, as ion concentration increased, consistent with increasing ion–ion interactions. Distinctive changes to water IR bands were related to Li^+ solvation and potential formation of solvent separated ion pairs. However, it is of note that ion pair formation is noted at concentrations where the rate of Fe dissolution was at a maximum, which suggests that this solution structuring did not significantly impact the electrochemical reaction over the concentration range below the $FeSO_4$ solubility limit.

Conflicts of interest

There are no conflicts to declare.

Data availability

The supporting data has been provided as part of the supplementary information (SI): S1 – experimental and literature data for Li_2SO_4 solutions molarity, pH, conductivity and viscosity; S2 – schematic of IR spectroelectrochemical cell; S3 – experimental data for determination of for ferrocyanide using cyclic voltammetry; S4 – full CV cycles for the experiments shown in Fig. 3; repeat CV measurements at fresh Fe electrodes; consecutive CV cycles (1–5) for Fe oxidation; S5 – *in situ* IR spectra for Fe dissolution in electrolytes of different concentrations. See DOI: https://doi.org/10.1039/d6cp00537c.

Acknowledgements

Hind A. Al-Malki acknowledges Umm Al-Qura University in the Kingdom of Saudi Arabia for PhD studentship funding.

References

1 H. Zhang and C. Sun, Cost-effective iron-based aqueous redox flow batteries for large scale energy storage application: A review, *J. Power Sources*, 2021, **493**, 229445.
2 J. Jiang and J. Liu, Iron anode-based aqueous electrochemical energy storage devices: Recent advances and future perspectives, *Interdiscip. Mater.*, 2022, **1**, 116–139.
3 S. Belongia, X. Wang and X. Zhang, Progresses and perspectives of all-iron aqueous redox flow batteries, *Adv. Funct. Mater.*, 2024, **34**, 2302077.
4 A. Dinesh, S. Olivera, K. Venkatesh, M. S. Santosh, M. G. Priya, Inamuddin, A. M. Asiri and H. B. Muralidhara, Iron-based flow batteries to store renewable energies, *Environ. Chem. Lett.*, 2018, **16**, 683–694.
5 L. W. Hruska and R. F. Savinell, Investigation of Factors Affecting Performance of the Iron-Redox Battery, *J. Electrochem. Soc.*, 1981, **128**, 18–25.
6 M. C. Tucker, A. Phillips and A. Z. Weber, All-iron redox flow batter tailored for off-grid portable applications, *ChemSusChem*, 2015, **8**, 3996–4004.
7 Z. He, F. Xiong, S. Tan, X. Yao, C. Zhang and Q. An, Iron metal anode for aqueous rechargeable batteries, *Mater. Today Adv.*, 2021, **11**, 100156.
8 X. Wu, A. Markir, Y. Xu, C. Zhang, D. P. Leonard, W. Shin and X. Ji, A rechargeable battery with an iron metal anode, *Adv. Funct. Mater.*, 2019, **29**, 1900911.
9 A. K. Manohar, K. M. Kim, E. Plichta, M. Hendrickson, S. Rawlings and S. R. Narayanan, A high efficiency iron-chloride redox flow battery for large-scale energy storage, *J. Electrochem. Soc.*, 2016, **163**, A5118–A5125.
10 K. L. Hawthorne, T. J. Petek, M. A. Willer, J. S. Wainwright and R. F. Savinell, An investigation into Factors Affecting

the Iron Plating Reaction for an all-iron flow battery, *J. Electrochem. Soc.*, 2015, **162**(1), A108–A113.
11 M. Pourbaix, *Atlas of electrochemical equilibria in aqueous solutions*, Pergamon, Oxford, 1966.
12 B. S. Jayathilake, E. J. Plichta, M. A. Hendrickson and S. R. Narayanan, Improvements to the coulombic efficiency of the iron electrode for an all-iron redox-flow battery, *J. Electrochem. Soc.*, 2018, **165**, A1630–A1638.
13 G. Horanyi, Investigation of the specific adsorption of HSO_4^-(SO_4^{2-}) and Cl^- ions on Co and Fe by radiotracer technique in the course of corrosion of the metals in perchlorate media, *Corros. Sci.*, 2004, **46**, 1741–1749.
14 J. Noack, M. Berkers, J. Ortner and K. Pinkwart, The influence of some electrolyte additives on the electrochemical performance of Fe/Fe^{2+} redox reactions for iron/iron redox flow batteries, *J. Electrochem. Soc.*, 2021, **168**, 040529.
15 S. Chai, J. Zhu, J. Jiang and C. M. Li, Elevating kinetics of passivated Fe anodes with NH_4Cl regulator: toward low-cost, long-cyclic and green cathode-free Fe-ion aqueous batteries, *Nano Res.*, 2022, **15**, 3187–3194.
16 S. Yu, X. Yue, J. Holoubek, X. Xing, E. Pan, T. Pascal and P. Liu, A low-cost sulfate-based all iron redox flow battery, *J. Power Sources*, 2021, **513**, 230457.
17 R. Chen, Redox flow batteries: Electrolyte chemistries unlock the thermodynamic limits, *Chem. – Asian J.*, 2023, **18**, e202201024.
18 B. Xue, X. Wu, Y. Guo, C. Zhang, W. Qian and L. Zhang, Review – Ionic liquids applications in flow batteries, *J. Electrochem. Soc.*, 2022, **169**, 080501.
19 https://www.chemicalbook.com/ProductChemicalPropertiesCB9232125_EN.htm.
20 L. Bamgbelu and K. B. Holt, *In Situ* Determination of pH at Nanostructured Carbon Electrodes Using IR Spectroscopy, *Materials*, 2019, **12**, 4044–4054.
21 M. M. Lounasvuori and K. B. Holt, Acid deprotonation driven by cation migration at biased graphene nanoflake electrodes, *Chem. Commun.*, 2017, **53**, 2351–2354.
22 A. Cartón, F. Sobrón, S. Bolado and J. I. Gerbolés, Density, Viscosity, and Electrical Conductivity of Aqueous Solutions of Lithium Sulfate, *J. Chem. Eng. Data*, 1995, **40**, 987–991.
23 C. Beriet and D. Pletcher, A microelectrode study of the mechanism and kinetics of the ferro/ferricyanide couple in aqueous media: the influence of the electrolyte and its concentration, *J. Electroanal. Chem.*, 1993, **361**, 93–101.
24 S. J. Konopka and B. McDuffie, Diffusion coefficients of ferri- and ferrocyanide ions in aqueous media, using twin-electrode thin-layer electrochemistry, *Anal. Chem.*, 1970, **42**, 1741–1746.
25 M. R. Wright, *An Introduction to Aqueous Electrolyte Solutions*, Wiley, 2007.
26 W. Wachter, S. Fernandez, R. Buchner and G. Hefter, Ion association and hydration in aqueous solutions of LiCl and Li_2SO_4 by dielectric spectroscopy, *J. Phys. Chem. B*, 2007, **111**, 9010–9017.
27 S. D. Fried and S. G. Boxer, Measuring Electric Fields and Noncovalent Interactions Using the Vibrational Stark Effect, *Acc. Chem. Res.*, 2015, **48**, 998–1006.
28 H. H. Adler and P. F. Kerr, Variations in Infrared spectra, molecular symmetry and site symmetry of sulfate minerals, *Am. Mineral.*, 1965, **50**, 132–147.
29 N. Kitadai, T. Sawai, R. Toniue, S. Nakashima, M. Katsura and K. Fukushi, Effects of ions on the OH stretching band of water as revealed by ATR-IR spectroscopy, *J. Solution Chem.*, 2014, **43**, 1055–1077.
30 G. E. Walrafen, Raman spectral studies of the effects of solutes and pressure on water structure, *J. Chem. Phys.*, 1971, **55**, 768–792.
31 Z.-F. Wei, Y.-H. Zhang, L.-J. Zhao, J.-H. Liu and X.-H. Li, Observation of the first hydration layer of isolated cations and anions through the FTIR-ATR difference spectra, *J. Phys. Chem. A*, 2005, **109**, 1337–1342.
32 K. J. Tielrooij, N. Garcia-Araez, M. Boon and H. J. Bakker, Cooperativity in ion hydration, *Science*, 2010, **328**, 1006–1009.
33 R. M. Izatt, D. Eatough, J. J. Christensen and C. H. Bartholomew, Calorimetrically determined $\log K$, ΔH°, and ΔS° values for the interaction of sulphate ion with several bi- and ter-valent metal ions, *J. Chem. Soc. A*, 1969, 47–53, DOI: 10.1039/J19690000047.
34 C. H. Chio, S. K. Sharma and D. W. Muenow, Raman of the iron sulphide materials. Micro-Raman studies of hydrous ferrous sulfates and jarosites, *Spectrochim. Acta, Part A*, 2005, **61**, 2428–2433.